Photosensitizer fluorescence and singlet oxygen luminescence as dosimetric predictors of topical 5-aminolevulinic acid photodynamic therapy induced clinical erythema

Srivalleesha Mallidi
Sriram Anbil
Seonkyung Lee
Dieter Manstein
Stefan Elrington
Garuna Kositratna
David Schoenfeld
Brian Pogue
Steven J. Davis
Tayyaba Hasan

Photosensitizer fluorescence and singlet oxygen luminescence as dosimetric predictors of topical 5-aminolevulinic acid photodynamic therapy induced clinical erythema

Srivalleesha Mallidi,[a] Sriram Anbil,[a] Seonkyung Lee,[b] Dieter Manstein,[c] Stefan Elrington,[a] Garuna Kositratna,[c] David Schoenfeld,[d] Brian Pogue,[e] Steven J. Davis,[b] and Tayyaba Hasan[a],*

[a]Massachusetts General Hospital, Wellman Center for Photomedicine, Boston, Massachusetts 02114
[b]Physical Sciences Inc., Andover, Massachusetts 01810
[c]Massachusetts General Hospital, Department of Dermatology, Boston, Massachusetts 02114
[d]Massachusetts General Hospital, Biostatistics Department, Boston, Massachusetts 02114
[e]Dartmouth College, Thayer School of Engineering, Hanover, New Hampshire 03755

Abstract. The need for patient-specific photodynamic therapy (PDT) in dermatologic and oncologic applications has triggered several studies that explore the utility of surrogate parameters as predictive reporters of treatment outcome. Although photosensitizer (PS) fluorescence, a widely used parameter, can be viewed as emission from several fluorescent states of the PS (e.g., minimally aggregated and monomeric), we suggest that singlet oxygen luminescence (SOL) indicates only the active PS component responsible for the PDT. Here, the ability of discrete PS fluorescence-based metrics (absolute and percent PS photobleaching and PS re-accumulation post-PDT) to predict the clinical phototoxic response (erythema) resulting from 5-aminolevulinic acid PDT was compared with discrete SOL (DSOL)-based metrics (DSOL counts pre-PDT and change in DSOL counts pre/post-PDT) in healthy human skin. Receiver operating characteristic curve (ROC) analyses demonstrated that absolute fluorescence photobleaching metric (AFPM) exhibited the highest area under the curve (AUC) of all tested parameters, including DSOL based metrics. The combination of dose-metrics did not yield better AUC than AFPM alone. Although sophisticated real-time SOL measurements may improve the clinical utility of SOL-based dosimetry, discrete PS fluorescence-based metrics are easy to implement, and our results suggest that AFPM may sufficiently predict the PDT outcomes and identify treatment nonresponders with high specificity in clinical contexts. © *The Authors. Published by SPIE under a Creative Commons Attribution 3.0 Unported License. Distribution or reproduction of this work in whole or in part requires full attribution of the original publication, including its DOI.* [DOI: 10.1117/1.JBO.19.2.028001]

Keywords: photodynamic therapy; singlet oxygen luminescence; photosensitizer; fluorescence; 5-aminolevulinic acid; dosimetry.

Paper 130338RRR received May 13, 2013; revised manuscript received Dec. 5, 2013; accepted for publication Dec. 5, 2013; published online Feb. 6, 2014.

1 Introduction

5-Aminolevulinic acid (ALA) photodynamic therapy (PDT) represents a promising approach to treat distributed and refractory lesions in oncologic and cosmetic dermatology.[1–10] As with any therapeutic strategy, accurate monitoring of the pertinent factors which impact the deposited dose is critical for robust and predictable PDT outcomes.[2,11] In simplest terms, the PDT dose can be thought of as a product of the photosensitizer (PS) concentration and fluence.[12] However, the deposited PDT dose, and therefore the subsequent PDT efficacy, depends on several factors, including the amount of active PS at the target site, light parameters, and the reactive species generated by the PS that cause cytotoxic effect.[2,12–14]

Different approaches to monitor the delivered PDT dose have been evaluated in preclinical and clinical settings.[7,12,13,15–18] In particular, the PS fluorescence-based metrics, such as photobleaching, have been widely investigated due to the relative simplicity of detection and have served as a measure of the PDT dose.[12,15,19–23] Another PS fluorescence-based metric that has been investigated in context of preclinical ALA-PDT

is protoporphyrin (PpIX) re-accumulation post-PDT, defined as additional conversion of ALA to PpIX that occurs after irradiation.[15] Although photobleaching and PpIX re-accumulation may be valuable predictors of the PDT outcome, the discrete measurements of PS fluorescence that enable quantification of these parameters may not comprehensively reflect the complex photophysical and photochemical interactions that lead to the therapeutic effect.[12,24–28] For example, studies have shown that variations in the PS cellular localization may diminish its PDT activity but not affect its fluorescence emission.[12,29–31] Furthermore, photobleaching can occur through nonsinglet oxygen ($^1O_2$) mediated mechanisms.[25,27] Thus, the specific biophysical pathways that lead to changes in the PS fluorescence, as provided by the more convenient and often-used point measurements, may not correlate with the production of cytotoxic species that influence PDT outcome.[12,25,32,33]

Another PDT dose metric being explored by several groups is measurement of singlet oxygen luminescence (SOL). Generally, singlet oxygen ($^1O_2$) is thought to be an important mediator of the PDT cytotoxicity, though nonsinglet oxygen mediated pathways could also lead to similar PDT effects.[12,27] Singlet oxygen can be monitored through an optical detection of its luminescence at 1270 nm. Pioneering works by Niedre et al.,[34] Yamamoto et al.,[35] Lee et al.,[36] and Baier et al.[37]

*Address all correspondence to: Tayyaba Hasan, E-mail: thasan@mgh.harvard.edu

have demonstrated the technical feasibility of detecting $^1O_2$ luminescence (SOL) in preclinical models during PDT. These measurements correlated well with treatment outcome, suggesting that real-time SOL detection could serve as a useful clinical dosimetry tool. However, on-line detection and quantitation of the SOL for clinical implementation have been historically difficult due to the high reactivity of $^1O_2$ *in vivo*, its relatively low luminescence yield, and the need for complex instrumentation compatible with the clinical workflow.[13] We therefore suggest exploring a slightly different perspective on the use of the SOL measurements in PDT dosimetry using less complicated instrumentation: Discrete measurements of $^1O_2$ luminescence (DSOL). The DSOL indicates the amount of active PS that can convert $^3O_2$ to $^1O_2$ and could provide a direct measure of the potential deposited PDT dose.[13,15] The DSOL detection immediately before light irradiation was demonstrated to correlate with the phototoxic response in humans.[18] Several studies showed that the PDT and the PS photobleaching could occur through nonsinglet oxygen mediated pathways. Given the exploration of various dosimetry parameters and the complexities involved in the PDT mechanism, the prognostic utility of dose-metrics such as DSOL remains unclear, especially in comparison with widely employed discrete PS fluorescence-based dosimetry.

The present study hypothesized that the discrete PS fluorescence would provide a different dosimetric measure than DSOL and explores the prognostic utility of each of these approaches in predicting treatment response. This is because the PS fluorescence, without a full spectral analysis to distinguish between various aggregation states and localization sites of the PS, represents the proportion of PS able to emit fluorescence in the observed ranges. SOL on the other hand represents the active PS available to induce $^1O_2$ mediated cytotoxic effects.[2,12,14,29,30,36] Hence, the two approaches reflect the deposited PDT dose in a mechanistically distinct manner and could have different treatment prediction capability. To test this hypothesis, we compared the utility of PS fluorescence-based metrics, PpIX photobleaching [percent PpIX photobleached (PPP) and absolute fluorescence photobleaching metric (AFPM)] and PpIX re-accumulation post-PDT (PPR), with DSOL-based metrics, (DSOL counts pre-PDT and change in DSOL counts pre/post-PDT), in predicting erythema resulting from two different doses of clinical ALA-PDT. Linear regression and receiver operating characteristic (ROC) curve analyses revealed that in the clinical setting tested, the PS fluorescence-based metric AFPM exhibited the best correlation with PDT induced erythema and the highest area-under-the-curve (AUC) in the ROC analysis than all other tested dosimetric parameters.

2 Materials and Methods

2.1 Participant Selection

Twenty-six healthy subjects (22 females, 4 males, median age of 28.33 years) with Fitzpatrick skin types I-III were recruited.[38] Subjects were excluded if they were pregnant or nursing, had a history of photosensitive diseases, were taking any photosensitive medications, were unwilling to comply with the study protocols, had any dermatological conditions within the location of the study test sites, had any allergies to ALA formulation, DuoDerm (Convatec, Princeton, New Jersey), or any adhesives, had received laser irradiations within 6 months of the study, were participating in any confounding research or studies,

was an employee of any sites participating directly in the study, or exhibited any condition or laboratory value that, in the opinion of the investigator, would potentially affect response or participation in the study. Subjects gave written and informed consent to participate in all aspects of this study in compliance with the US Federal Code of Regulations pertaining to conduct of clinical studies (21CFR part 50 and 56). This study was conducted according to good clinical practice guidelines and the declaration of Helsinki, and was approved by the Institutional Review Board of Massachusetts General Hospital.

2.2 ALA Application

Six 2×2 cm^2 test sites on the inner arm were selected and outlined with permanent marker. Levulan® Kerastick® (DUSA Pharmaceuticals, Wilmington, Massachusetts) was topically applied to three test sites (Fig. 1, yellow boxes) using same number of application strokes. The vehicle content of the ALA formulation was applied to two sites (Fig. 1, gray boxes). One site received no treatments and served as control (Fig. 1).

2.3 Photodynamic Therapy

Light was delivered via fiber optic using a 635 nm diode laser at 50 mW/cm^2 (HPD7401, High Power Devices, North Brunswick, New Jersey). The beam was passed through a neutral density filter with a 2×2 cm^2 opening to facilitate irradiation only at the square shaped test site. Light delivery apparatus was placed 5 mm away from the skin surface. Eye protection was provided to subjects during light delivery. Irradiations were performed within American National Standards Institute (ANSI) standards, and all safety regulations regarding the use Class IIIB lasers were followed.

Three hours after the ALA application, two ALA treated sites received 5 J/cm^2 (A5 site), or 25 J/cm^2 (A25 site) light exposure at 50 mW/cm^2. Sites containing vehicle received no light (V_{only} site) or 25 J/cm^2 (V25 site). Erythema, fluorescence and the DSOL measurements were taken at time points (T) with the
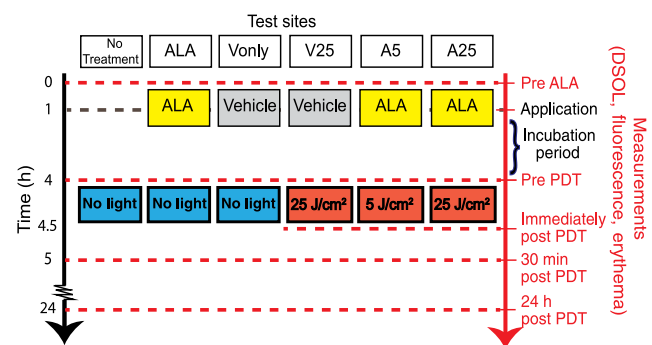
Fig. 1 Schematic of the clinical study workflow. The six test-sites on the upper inner arm of each subject are represented by the abbreviations no-treatment (site that did not receive ALA, vehicle, or irradiation), ALA (site that received ALA only), V_{only} (site that received only the vehicle solution of the ALA formulation), V25 (site that received vehicle solution and 25-J/cm^2 fluence at 50-mW/cm^2 irradiation), A5 (site that received ALA and 5-J/cm^2 fluence at 50-mW/cm^2 irradiation), and A25 (which received ALA and irradiation at 25-J/cm^2 fluence at 50-mW/cm^2 irradiation). Black arrow indicates the timeline of the study. Red arrow indicates the time-points at which measurements (DSOL, fluorescence, and erythema) and photographs were taken. Immediately post-PDT, measurements and photographs were only taken at the sites that received light irradiation.

following subscripts: Pre-ALA (before ALA application), Pre-PDT (3 h after application of ALA and prior to PDT), post-PDT (immediately post-PDT), 30 min post-PDT and 24 h (24 h post-PDT).

2.4 Singlet Oxygen ($^1O_2$) Measurements

The *in vivo* SOL detection system is previously described in detail.[18,36,39,40] Briefly, the system consists of (i) a 635-nm diode laser module; (ii) optical filters/PMT detection system; and (iii) data acquisition system with a photon counting board. This device uses two separate optical fibers to deliver excitation light and collect $^1O_2$ luminescence emission. The excitation light with a bandpass filter to further eliminate near-IR light leakage from the excitation diode laser was delivered to the test site with the beam size of 15 mm in diameter by an optical fiber with a collimator. A 3-mm liquid light guide was used to collect the near-IR emission. The detection fiber optics was set at a 40 deg angle from the excitation fiber optics. This modification to the system was done to minimize signal variations due to heterogeneous accumulation of PpIX in test subjects, if any, by a exposing larger area for both light excitation and singlet O_2 signal collection. For the ALA-induced PpIX excitation, a fiber coupled diode laser with the wavelength centered at 635 nm was operated at a repetition rate of 10 kHz with a pulse width of 5 μs with an average intensity of 4.3 mW/cm^2. The $^1O_2$ phosphorescence signal was detected and analyzed using automated computer software. Spectral and temporal discrimination techniques were used to isolate the DSOL from the PS fluorescence. Spectral discrimination was performed via a set of three optical filters (centered at 1220, 1270, and 1320 nm; FWHM = 15 nm) i.e., the two signals obtained with filters centered at 1220 and 1320 nm provided measurements of the background emission that did not contain singlet O_2 emission, while the signals collected at 1270 nm contained singlet oxygen emission with background emission. The singlet oxygen counts were calculated by subtracting the background (average of photon counts from 1220- and 1320-nm signal) from the 1270-nm photon counts. Temporal discrimination was achieved through the lifetime difference between short-lived PS fluorescence and longer-lived SOL as has been previously reported. Briefly, the fluorescence signal is observed when the excitation laser is "on" between 6 and 11 μs (5-μs pulse width) after the start of data acquisition. The longer-lived singlet oxygen signal that persists even after switching off the excitation laser is considered for calculating the SOL photon counts. The SOL counts are calculated using the formula

$$^1O_2 \text{ counts} = \text{sum}[1270 \text{ nm}(t_1 : t_2)]$$
$$- \frac{\text{sum}[1220 \text{ nm}(t_1 : t_2)] + \text{sum}[1320 \text{ nm}(t_1 : t_2)]}{2}, \quad (1)$$

where t_1 and t_2 represent 11.3 and 30 μs, respectively. Four $^1O_2$ measurements (signal accumulated for 80,000 laser shots for each measurement) were taken per test site.

2.5 PpIX Fluorescence Measurements

PpIX photobleaching in tissue was monitored with a system for *in vivo* fluorescence detection at 670 nm provided by Aurora Optics, Inc (Hanover, New Hampshire).[24,28,39,41–44] The system consisted of three parts. The first part is a continuous wave 405-nm diode laser to excite PpIX. The second part is a fiber optic probe to deliver the excitation light and collect the fluorescent light *in vivo*. The fiber probe (Aurora Optics, Inc., Hanover, New Hampshire), was composed of one excitation fiber (100 μm) surrounded by six 100-μm detection fibers. The construction of the probe involves insertion of the seven 100-μm fibers into a 21-gauge needle and securing it using a low fluorescence epoxy. The opposite end of the fiber probe is bifurcated into the single source fiber and a bundle containing the six detection fibers. These are each connected to the laser source and the PMT detector, respectively. As previously reported,[24,28,41] this configuration of the fiber probe can be used for quantitative fluorescence measurements with reduced background absorption effects as it measures fluorescence from regions of tissue that are smaller than the average scattering length of the tissue. The third part of the system is the fluorescence light detector R928 Hamamatsu PMT (Hamamatsu Photonics, Shimokanzo, Japan) coupled to a 600-nm long-pass filter to detect PpIX fluorescence. A chopper wheel (Ithaco, Ithaca, New York) equipped with a light emitting diode (LED)-photodiode provided a triggering frequency of 500 Hz and was used to cycle the excitation light on and off to allow lock-in detection of the fluorescence signal. The fiber optic was placed in gentle contact with the skin and nine fluorescence measurements were taken across each test site and averaged. Fluorescence emission was analyzed and recorded using custom-designed LabVIEW software (National Instruments, Austin, Texas).

2.6 Erythema Measurements

Erythema was measured via DermaSpectometer DSM II ColorMeter (Cortex Technology, Hadsund, Denmark). The probe was placed in gentle contact with the test site and three measurements were taken at left, center and right areas of the test site. At various time points, erythema from same regions within the test site was obtained.

2.7 Study Procedure

The study consisted of three visits. During the first visit, subjects were screened per the inclusion and exclusion criteria in the institutional review board (IRB) protocol, and enrolled in the study after providing informed consent. During the second visit, ALA was administered to test sites and a nonadherent bandage was applied between measurements to protect the site from ambient light and prevent drug leakage. Measurements were taken and PDT was administered as indicated (Fig. 1). The third visit consisted of a follow up measurements taken at 24 h post treatment.

2.8 Blinded Erythema Evaluation

A panel of six dermatologists evaluated photographs (normal and cross-polarized with a color scale taken using Nikon D90, Nikon, Tokyo, Japan) of each individual test site for intensity of erythema. The dermatologists were blinded to the treatment conditions and subject information. A scale of 0 to 3, representing, no erythema, mild, moderate and intense erythema respectively was used for erythema evaluation.[45,46] For each test site, the average of the erythema scores given by the six dermatologists was calculated and utilized for statistical analysis.

2.9 Statistical Analysis

Statistical analysis was performed using Statistical Analysis System (SAS) Institute Inc. (Cary, North Carolina), Graphpad

Prism (La Jolla, California), and MedCalc (Ostend, Belgium). The dose-response curves were analyzed by repeated measures mixed model linear regression. Statistical comparisons were performed via two-tailed paired student's t-test ($p < 0.05$ was considered significant unless specified). The dosimetric parameters' performance was investigated using the ROC analysis, in which test sites that received PDT were assigned to either a responder or a nonresponder group based on the blinded dermatologists erythema evaluation of the test site photographs. Sites that received an erythema score of 0 were allocated to the nonresponding group and test sites that received a score of 1, 2, or 3 (representing mild, moderate, and intense erythema) were allocated to the responding group. The ROC analysis was performed using MedCalc (Ostend, Belgium) software. Specifically, the standard error of the AUC and pairwise ROC curve comparison were performed using the DeLong et al.[47] method. The optimal cut-off point (maximum Youden index)[48] where separation between false positives and false negatives is maximum and the corresponding sensitivity and specificity was also calculated with MedCalc.

3 Results and Discussion

3.1 Phototoxic Response Correlated with PDT Light Dose

Erythema measured post-PDT was caused by inflammation due to phototoxicity.[1] Mean erythema measured at $T_{\text{pre-ALA}}$ with

dermspectrometer was 8.4 (0.73 S.E.M) and exhibited a coefficient of variation (COV) of 8.6%. All of the control sites (V_{only}, V25, and no-treatment) exhibited no significant increase in mean erythema at the $T_{\text{pre-ALA}}$ [start of the study, Fig. 2(a) blue bars] and $T_{24\,h}$ [end of the study, Fig. 2(a) red bars] time point in the study ($p > 0.5$). Mean erythema score of all the test sites given by the dermatologists at $T_{\text{pre-ALA}}$ was 0.05 (0.005 S.E.M) and there was no significant difference between the test sites at $T_{\text{pre-ALA}}$.

Moderate agreement, established via Fleiss kappa statistics ($k = 0.5911$, $r^2 = 0.727$, p-value <0.0001), was observed between erythema readings obtained from blinded reviewers' evaluation of photographs and those obtained from the derm-spectrometer [Fig. 3(a)]. Figure 3(b) represents the average of the blinded erythema scores in the test sites at various time points. At $T_{\text{pre-ALA}}$, there was no significant difference between erythema scores of V25, A5, and A25 sites [Fig. 3(b), blue bars]. At $T_{24\,h}$, A5, and A25 sites had significantly higher erythema than the V25 test site [Fig. 3(b), red bars]. Both the dermspectrometer and blinded evaluation significantly indicated a higher mean phototoxic response in the A25 site [Figs. 2(b) and 3(b) respectively] versus the A5 site. Correlations between the dosimetry parameters and PDT-induced phototoxicity were performed using dermspectrometer erythema readings.

One subject discontinued the study during the PDT treatment. The change in erythema from $T_{\text{pre-ALA}}$ to $T_{24\,h}$ is depicted
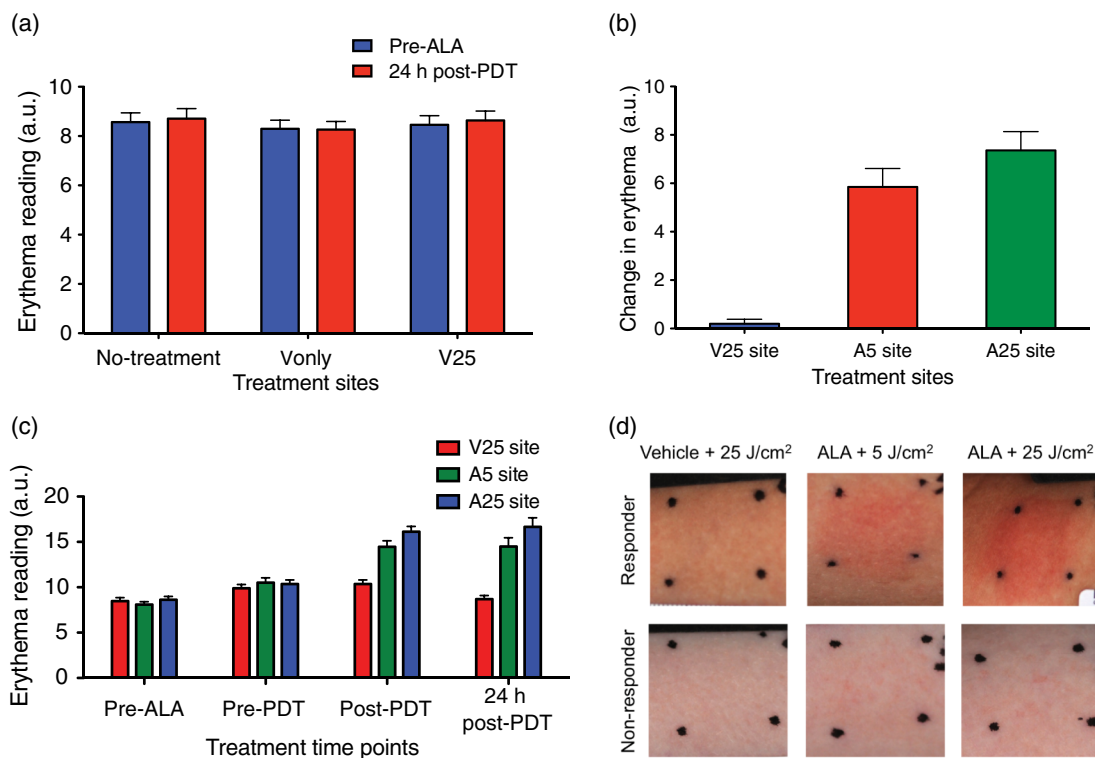

Fig. 2 Erythema measurements and PDT response-based classification of subjects (a) The control sites (no-treatment, V_{only} and V25 sites) exhibited no significant difference ($p < 0.001$) in erythema from $T_{\text{pre-ALA}}$ (blue bars) to $T_{24\,h}$ (red bars) for 25 subjects. (b) Change in erythema between $T_{\text{pre-ALA}}$ and $T_{24\,h}$ is plotted for the V25 (blue), A5 (red), and A25 (green) sites ($n = 25$ subjects). The A25 site exhibited significantly greater erythema than the A5 site ($p < 0.01$). (c) Average erythema scores taken from the V25, A5, and A25 sites at various time points ($n = 25$ subjects). The A5 and A25 sites exhibited a significant increase in erythema from $T_{\text{pre-PDT}}$ to $T_{\text{post-PDT}}$. (d) Representative photographs of test sites taken at $T_{24\,h}$ from a PDT responder and a nonresponder. The A25 site exhibits visibly greater erythema than the A5 site in the responder. Very little difference in erythema is apparent amongst all sites in the nonresponder. Error bars indicate S.E.M.

for the remaining 25 subjects in Fig. 2(b). Erythema increased by 72% (8.4% S.E.M.) and 85.3% (8.5% S.E.M.) at A5 and A25 sites, respectively from $T_{\text{pre-ALA}}$ to $T_{24\text{ h}}$ [red and green bars, Fig. 2(b)]. Erythema readings obtained at the three light treated sites (V25, A5, and A25 sites) at various time points during the study is shown in Fig. 2(c). A 25% increase in erythema was observed at all test sites from $T_{\text{pre-ALA}}$ to $T_{\text{pre-PDT}}$ [Fig. 2(c)]. This was likely due to the bandage that was applied to all subjects, which served to protect test sites from ALA leakage and ambient light. However, only the A5 [Fig. 2(c), green bars] and A25 [Fig. 2(c), blue bars] sites exhibited a significant increase in erythema at $T_{\text{post-PDT}}$ and $T_{24\text{ h}}$ ($p < 0.05$), suggesting that the post-PDT increase in erythema observed at the ALA-PDT sites was due to phototoxicity. Representative photographs depicting typical treatment responding and nonresponding subjects in the three light treated sites (V25, A5, and A25) at $T_{24\text{ h}}$ are shown in Fig. 2(d). The photographs visibly show intense erythema in the PDT treated sites of the responding subject. The nonresponding subject had very minimal erythema in the test sites. These observations are consistent with previous studies that characterized erythema after ALA-PDT.[3,49] Based on our results and literature,[1,3,18,49] we selected erythema scores at $T_{24\text{ h}}$ as the parameter

most indicative of PDT treatment response, and subsequently correlated these scores with all dosimetric measurements.

3.2 Conversion of ALA to PpIX in the Test Sites

Average fluorescence measurements taken at various time points are shown for 25 subjects at all test sites in Fig. 4(a). Baseline fluorescence observed at $T_{\text{Pre-ALA}}$ is a combination of background autofluorescence and signals from endogenous porphyrins in the skin [Fig. 4(a), blue bars].[50,51] Baseline fluorescence COV for 25 subjects was 9.93% (0.79% S.E.M). The ALA, A5, and A25 sites exhibited a significant increase ($p < 0.0001$) in fluorescence from $T_{\text{pre-ALA}}$ [Fig. 4(a), blue bars] to $T_{\text{pre-PDT}}$ [Fig. 4(a), red bars], while the V_{only} and V25 sites exhibited no significant increase in fluorescence over this time period. Amongst the 25 subjects, 22 subjects exhibited a 252% (100% S.E.M) increase in the PpIX fluorescence at the ALA, A5, and A25 sites. The other three subjects, who exhibited less than a 5% increase in dermspectrometer measurement of erythema from $T_{\text{pre-PDT}}$ to $T_{\text{post-PDT}}$, had a 49.8% increase in PpIX fluorescence at the ALA treated sites. Although the three subjects had fivefold less increase in PpIX fluorescence compared to the cohort, they were considered in all statistical analyses unless mentioned specifically.
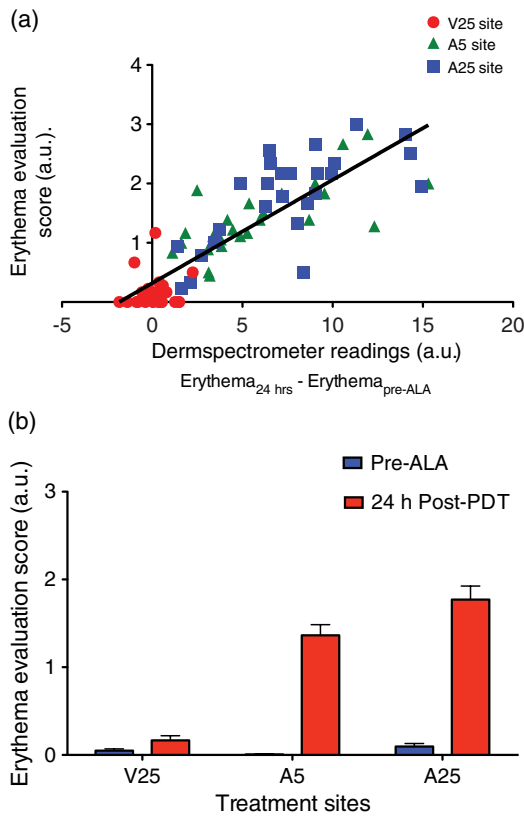
Fig. 3 Blinded dermatologists' erythema evaluation score and dermspectrometer readings have good correlation. (a) A significant linear correlation (black line) was observed between erythema scores obtained from the blinded dermatological evaluation and those taken by the dermspectrometer ($r^2 = 0.727$, $p < 0.05$, $n = 25$ subjects). Data from three light treated sites (V25, A5, and A25 treatment sites) for 25 subjects were considered in this analysis. (b) Average erythema scores given by the dermatologists on the V25, A5, and A25 sites for $n = 25$ subjects at time point $T_{\text{pre-ALA}}$ and $T_{24\text{ h}}$. There was significant difference between the A5 and A25 sites erythema scores (p-value <0.05).
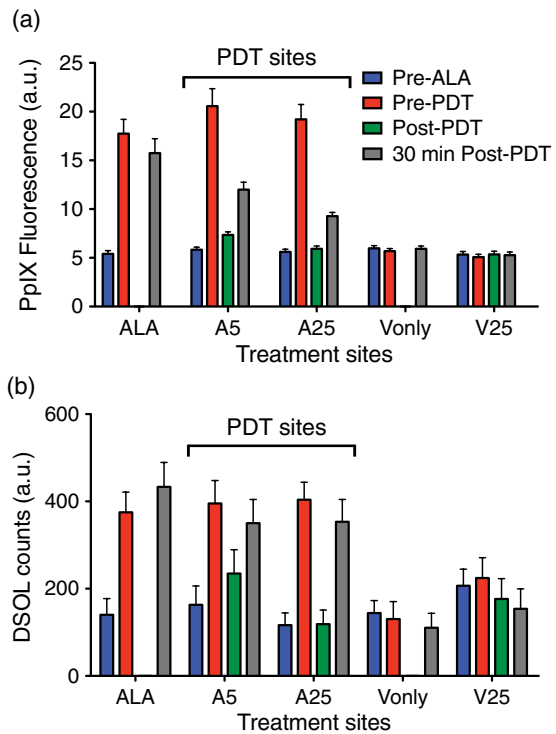
Fig. 4 PS-fluorescence and DSOL counts are PDT dose dependent. (a) PpIX fluorescence, and (b) DSOL counts taken at the ALA, A5, A25, V_{only}, and V25 sites are plotted at the $T_{\text{pre-ALA}}$ (blue), $T_{\text{pre-PDT}}$ (red), $T_{\text{post-PDT}}$ (green), and $T_{30\text{ min post-PDT}}$ (gray) time-points ($n = 25$ subjects). An increase in PpIX fluorescence and DSOL counts was observed from $T_{\text{pre-ALA}}$ to $T_{\text{pre-PDT}}$ only at the ALA, A5, and A25 sites. PpIX photobleaching and change in DSOL counts was observed from $T_{\text{pre-PDT}}$ to $T_{\text{post-PDT}}$ at the A5 and A25 sites. PpIX re-accumulation was also observed at these sites from $T_{\text{post-PDT}}$ to $T_{30\text{ min post-PDT}}$. Error bars indicate S.E.M.

3.3 PS Photobleaching was PDT Dose Dependent

The PS fluorescence-based dosimetry has proven useful in both preclinical and clinical settings.[19,45,52–56] In accordance to literature, we also observed that PpIX fluorescence decreased significantly in both PDT-treated sites [Fig. 4(a) red and green bars in the A5 and A25 test sites]. Two photobleaching parameters, namely percentage of PpIX photobleached due to PDT (PPP) and AFPM were calculated from the discrete fluorescence measurements taken at time points $T_{\text{pre-ALA}}$, $T_{\text{pre-PDT}}$, and $T_{\text{post-PDT}}$ as shown in Eqs. (2) and (3), respectively. The percent change in PpIX fluorescence due to PDT (PPP) is defined as

$$PPP = 100$$
$$\times \frac{(PpIX_{\text{pre-PDT}} - PpIX_{\text{pre-ALA}}) - (PpIX_{\text{postPDT}} - PpIX_{\text{pre-ALA}})}{PpIX_{\text{pre-PDT}} - PpIX_{\text{pre-ALA}}}. \quad (2)$$

The AFPM parameter is defined as

$$AFPM = (PpIX_{\text{pre-PDT}} - PpIX_{\text{pre-ALA}})$$
$$- (PpIX_{\text{post-PDT}} - PpIX_{\text{pre-ALA}}). \quad (3)$$

The PPP was significantly greater in the A25 sites than the A5 sites [Fig. 4(a), paired t-test, $p < 0.05$]. The average PPP value for 25 subjects was 86.58% (3.1% S.E.M) and 98.7% (4.7% S.E.M) in the A5 and A25 test sites, respectively. There was no significant change in fluorescence at the V25 test site post light exposure [Fig. 4(a)]. The average AFPM values for 25 subjects were 13.2 F.U. (Fluorescence Units) with 1.7 S.E.M and 13.3 F.U. with 1.5 S.E.M. in the A5 and A25 test sites, respectively. There was no significant difference in the AFPM values between the two treatment groups. Here, we observe that the PPP was light dose dependent (i.e., higher PPP was observed for the A25 site), while the AFPM parameter does not correlate with light dose (No significant difference between A5 and A25 sites). There was no significant linear correlation between the percent of PpIX photobleached and percent increase in PpIX fluorescence between $T_{\text{pre-ALA}}$ and $T_{\text{pre-PDT}}$ [Fig. 5(a), $r^2 = 0.002$, $p > 0.5$], where percent increase

in PpIX fluorescence (PIPF) was defined by Eq. (4). The PIPF represents the ALA to PpIX conversion capability of the subject.
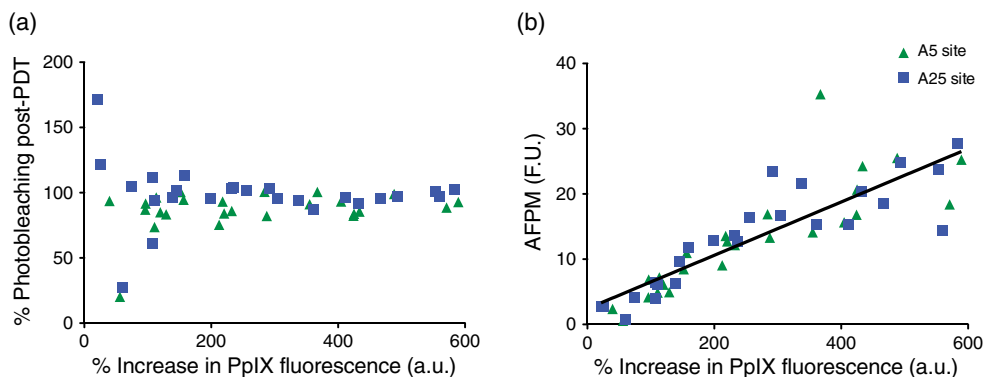
$$\%\text{Increase in } PpIX \text{ fluorescence(PIPF)}$$
$$= 100 \times \frac{PpIX_{\text{pre-PDT}} - PpIX_{\text{pre-ALA}}}{PpIX_{\text{pre-ALA}}}. \quad (4)$$

The AFPM measures the absolute amount of PS that is photobleached and accounts for the amount of PS present at the treatment site prior to PDT.[45,57] A significant linear correlation was observed between AFPM and PIPF [Fig. 5(b), $r^2 = 0.74$, $p < 0.0001$]. These results demonstrate that PPP is independent of initial PPIX concentration whereas AFPM is dependent on the initial PpIX concentration.

The clinical data presented here are consistent with pre-clinical mice work presented by Zeng et al.[45] where the PPP correlated with light dose and AFPM correlated with treatment response respectively. The PPP score does not account for the amount of the PS present at the treatment site prior to PDT, i.e., in this study most of the PS photobleached during PDT in test sites that had higher or lower PpIX at $T_{\text{pre-PDT}}$. This effect is more prominent at low PpIX levels, as those occurring *in vivo*, where most of the PS is photobleached.[57] It should be noted that PPP is independent of device specifications and the PPP range determined in a particular study could be translated to other clinical investigations. On the other hand AFPM values are device specific, e.g., the change in PMT sensitivity, etc., can change the AFPM values obtained, thereby making comparisons between various clinical investigations difficult. However, in a given cohort of subjects and fluorescence detection device, the AFPM might be a better dosimetry parameter than PPP.

3.4 Post-PDT Re-accumulation of PpIX Correlated with AFPM

The PpIX fluorescence increased from $T_{\text{post-PDT}}$ [Fig. 4(a), green bars] to $T_{\text{30 min post-PDT}}$ [Fig. 4(a), gray bars] at the PDT-treated sites (A5 and A25 sites). No significant change in fluorescence was detected in sites that did not receive ALA (V_{only} and V25 sites). Star et al.[14] suggested that only 3.6% of ALA is converted to PpIX in a 3- to 4-h incubation period. These results indicate

Fig. 5 Percent PpIX photobleached (PPP) is independent of the percent increase in PpIX fluorescence (PIPF) at $T_{\text{pre-PDT}}$, while Absolute fluorescence photobleaching metric (AFPM) is dependent on PIPF. Scatter plot of (a) percent increase in PpIX fluorescence at $T_{\text{pre-PDT}}$ (PIPF) and PPP and (b) PIPF and AFPM at A5 (green triangles) and A2 (blue squares). There was no significant linear correlation between PIPF and PPP ($r^2 = 0.002$, $p > 0.5$). A significant linear correlation was observed between AFPM and PIPF [Fig. 5(b), $r^2 = 0.74$, $p < 0.0001$].

that after PpIX photobleaching due to laser irradiation, residual ALA continues conversion to PpIX in viable cells with intact heme-synthesis.[14,15] This phenomenon is generally termed re-synthesis or re-accumulation. Generally, tissues that exhibit greater PpIX photobleaching also exhibit less PpIX re-accumulation.[15] Studies on pig skin have demonstrated that the percentage of PpIX re-accumulated at the treatment site is inversely proportional to the light fluence delivered.[20] In this study, the PpIX that re-accumulated (PPR) post PDT as a ratio of initial increase in PpIX at pre-ALA time point was defined as

%PpIX re-accumulation(PPR)

$$= 100 \times \frac{PpIX_{30 \text{ min post-PDT}} - PpIX_{post-PDT}}{PpIX_{pre-PDT} - PpIX_{pre-ALA}}. \quad (5)$$

In accordance with de Bruijn et al.[15] and Thissen et al.,[20] we demonstrate in human skin that re-accumulation of PpIX is fluence dependent. The PPR values were 31.6% (4.2% S.E.M) and 25.2% (2.2% S.E.M) at the A5 and A25 sites, respectively in the 22 subjects (excluded three subjects from the 25 subjects that had less than 50% increase in PpIX fluorescence at $T_{pre-PDT}$). The A5 site that received a low light dose had significantly greater PpIX re-accumulation compared to A25 test site. The $V25$ and V_{Only} sites exhibited no significant change in PpIX fluorescence from $T_{pre-PDT}$ [Fig. 4(a), red bars] to $T_{30 \text{ min post-PDT}}$ [Fig. 4(a), gray bars]. For the ALA-PDT treated sites, we observed a significant non-zero correlation between PpIX photobleaching parameters AFPM and PPR (Fig. 6, $r^2 = 0.23$, p-value <0.005) which indicated that the greater the PpIX photobleaching, the lower the PpIX re-accumulation.

3.5 Singlet Oxygen Luminescence Counts Correlated with the PS Fluorescence

Average DSOL measurements taken at various time points for 25 subjects are shown [Fig. 4(b)]. There was no significant difference in DSOL measurements between any of the test sites at $T_{Pre-ALA}$ [Fig. 4(b), blue bars]. Baseline DSOL measurements observed before the application of ALA is likely due to the $^1O_2$ generation from naturally occurring endogenous porphyrins.[50,51] The ALA, A5, and A25 sites exhibited a significant increase in DSOL counts from $T_{pre-ALA}$ [Fig. 4(b), blue bars] to $T_{pre-PDT}$ [Fig. 4(b), red bars] indicating the presence of active
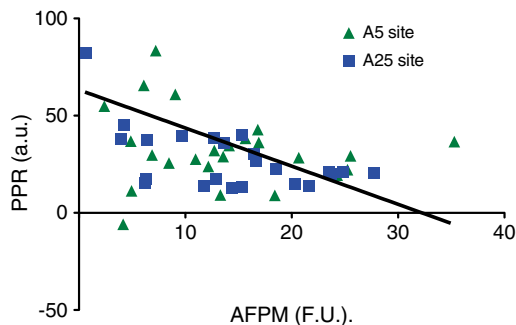
Fig. 6 Greater the PpIX photobleaching, lesser the PpIX re-accumulation. A significant linear correlation (black line) was observed between AFPM and percent PpIX re-accumulation (PPR) post-PDT ($r^2 = 0.83$, $p < 0.05$, $n = 25$ subjects). As the delivered fluence was increased (A5 versus A25 sites), a greater percentage PpIX photobleaching was observed with concomitantly lower PpIX re-accumulation. F.U. stands for fluorescence units.

PpIX able to convert $^3O_2$ to $^1O_2$ ($p < 0.0001$ for ALA, A5, and A25 sites). The DSOL counts taken at the $T_{pre-PDT}$ [Fig. 4(b), red bars] time point are subsequently referred to as DSOL counts pre-PDT. The V_{only} and V25 sites exhibited no significant increase in DSOL counts from $T_{pre-ALA}$ to $T_{pre-PDT}$ [Fig. 4(b)].

$^1O_2$ generation at a given depth z and time point t is thought to be related to the product of the active PS concentration (PS) at the site, ground state molecular oxygen concentration ($^3O_2$) at the site (available either due to diffusion from environment or via vascular perfusion), and fluence Φ and can be generalized by the equation

$$^1O_2(z, t) \propto [PS(z, t)][^3O_2(z, t)]\Phi(z, t). \quad (6)$$

In the present study $^3O_2$ in the epidermis layer was likely similar before and 3 h after application of the ALA primarily due to diffusion of oxygen from the environment. As the PDT treatment progresses, hypoxia could occur at depth of 0.2 to 1 mm.[57–59] Beyond 1 mm plenty of oxygen is available for the PDT action via vascular perfusion. A minor increase in erythema due to the bandage was observed at time point $T_{pre-PDT}$ (3 h after application of ALA). This minor increase in erythema could cause an increase in oxygen supply to the dermis. However, it should be noted that this increase at erythema at $T_{pre-PDT}$ is similar in all the control and light-treated test sites and hence any effects on DSOL measurements due to this minor increase in molecular oxygen can be considered constant amongst all our test sites. Given the absence of change in $^3O_2$, the DSOL measurements were likely proportional to the active PpIX concentration at the test site when the same fluence was delivered.

A recent simulation study by Liu et al.[57] and an *in-vitro* study by Dysart et al.[60] showed that $^1O_2$ dose is determined solely by the initial PS concentration. To gauge the effect of the initial PS concentration [PIPF, Eq. (4)] on the treatment efficacy, we correlated the percentage increase in PpIX fluorescence 3 h post ALA application (PIPF) with the corresponding increase in DSOL counts 3 h post-ALA application [Eq. (8)].

Increase in DSOL counts = DSOL counts$_{pre-PDT}$

$$- DSOL counts_{pre-ALA}. \quad (7)$$

We observed a linear correlation ($r^2 = 0.34$, p-value <0.001) between the DSOL counts and PIPF [Fig. 7(a)]. In addition, we also observed that test sites having higher PpIX fluorescence and DSOL counts had higher erythema [Fig. 7(b)]. These results indicate that initial PS concentration and corresponding DSOL counts that represent the active PS in the location could act as dosimetry parameters. In the following sections we compared the increase in DSOL counts termed as "DSOL counts pre-PDT" to the widely used PS photobleaching dose-metric.

A significant decrease in DSOL counts from $T_{pre-PDT}$ [Fig. 4(b), red bars] to $T_{post-PDT}$ [Fig. 4(b), green bars] was observed at the A5 and A25 sites ($p < 0.01$). The V_{only} and the V25 sites exhibited no significant difference in DSOL counts over this period. A significant increase in DSOL counts was observed at the A5 and A25 sites from $T_{post-PDT}$ [Fig. 4(b), green bars] to $T_{30 \text{ min post-PDT}}$ [Fig. 4(b), gray bars], indicating re-accumulation of PpIX at these test sites [p < 0.01]. The decrease in DSOL counts from $T_{pre-PDT}$ [Fig. 4(b), red bars] to $T_{post-PDT}$ [Fig. 4(b), green bars] was termed as change in DSOL counts [Eq. (8)] and was considered as a dosimetric parameter that is comparable to the PS photobleaching AFPM parameter.
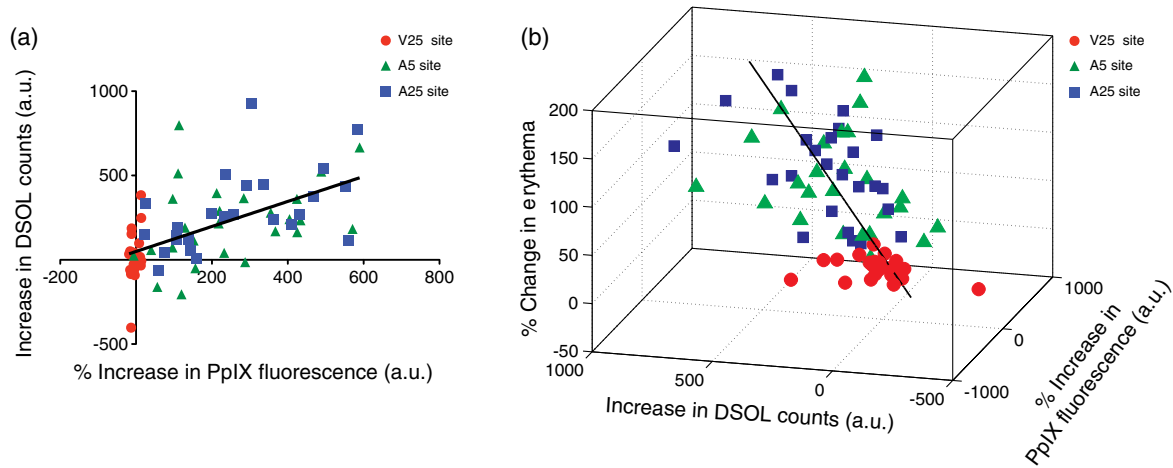
Fig. 7 (a) Scatter plots illustrating the relationship between increase in DSOL counts and PpIX fluorescence 3-h post ALA application in three light-treated test sites namely V25 site (red circles), A5 site (green triangles) and A25 site (blue squares). Each data point on the graph represents a test site. Data for 25 subjects is shown here. (b) Three-dimensional scatter plot illustrating relationship between (1) increase in DSOL counts, (2) % increase in PpIX fluorescence 3 h after ALA application, and (3) percentage change in erythema observed in the subjects at the respective test sites post light-treatment. The solid black line represents significant non-zero linear regression with r^2 values 0.34 and 0.6, respectively for both the plots.

$$\text{Change in DSOL counts} = \text{DSOL counts}_{\text{pre-PDT}}$$
$$- \text{DSOL counts}_{\text{post-PDT}}. \qquad (8)$$

Both the DSOL counts pre-PDT (a dosimetric parameter that indicates the initial amount of active PpIX), and the change in DSOL counts pre/post-PDT (which indicates the change in the amount of active PpIX resulting from PDT), were evaluated for their ability to predict PDT induced phototoxicity.

3.6 Prognostic Utility of PS Fluorescence-Based Metrics and DSOL-Based Metrics, in Predicting PDT-Induced Phototoxicity

Significant, non-zero, correlations were established between the dosimetric parameters PPR, AFPM, and DSOL counts pre-PDT (Table 1). The PPP parameter and change in DSOL counts pre/

Table 1 Correlation statistics between erythema measured at $T_{24\,h}$ and the dosimetric parameters tested in the study. All correlations were determined using linear mixed model analysis. $N = 25$ subjects for each correlation. Amongst the five dosimetric parameters, AFPM had greater correlation with the PDT-induced erythema. "NS" indicates no significant while "S" indicates a significant difference.

Parameter	Slope	95% Confidence Intervals	r^2	Is slope significantly non-zero? P-value
PPP	0.067	−0.073 to 0.21	0.019	0.34 (NS)
AFPM	0.14	0.10 to 0.18	0.54	<0.0001 (S)
PPR	−0.25	−0.47 to −0.034	0.10	0.02 (S)
DSOL counts pre-PDT	1.98	0.48 to 3.5	0.13	0.0106 (S)
Change in DSOL counts	1.36	−0.69 to 3.4	0.036	0.1880 (NS)

post-PDT did not have a significant correlation with erythema. Figure 8 shows dosimetry parameters plotted against erythema evaluated by dermspectrometer in the A5 (green triangles) and A25 (blue squares) sites that received PDT treatment. Solid black lines in the graphs [Figs. 8(b)–8(d)] indicate a significant and non-zero linear regression fit. The dotted black line in Figs. 8(a) and 8(e), shows the linear regression fit, however, the slope is not significantly different from zero. Overall, AFPM had greater correlation with PDT-induced erythema than other metrics ($r^2 = 0.54$).

The clinical utility of a dosimetric parameter depends on its ability to predict the extent of therapeutic efficacy, as well its ability to classify patients as treatment responders or nonresponders. We performed the ROC analysis on the dosimetry parameters that had significant nonzero correlation with erythema (Fig. 9). The AFPM exhibited the highest AUC (Table 2). There was a significant difference between the ROC curves of the AFPM and DSOL counts pre-PDT dosimetry parameters). Furthermore, the best cut-off on the ROC curve for distinguishing the responders from the nonresponders was identified (i.e., maximum separation between the false positives and false negatives) for each dosimetry parameter using Youden index maximization algorithm.[61] Circles on the ROC curve in Fig. 9 represent the optimal cut-off point. At this cut-off point, AFPM had a sensitivity of 61.5% and specificity 100%, while the DSOL counts pre-PDT parameter had a sensitivity of 79.5% and specificity of 72.7%, respectively. The DSOL counts pre-PDT had higher sensitivity than AFPM at the optimal cut-off point. This result was encouraging and offered support to our hypothesis that DSOL counts pre-PDT might be more sensitive in detecting the active PS that causes phototoxicity and thereby aid in correctly identifying treatment responders. However, the choice of using a particular dosimetric method needs to be made according to the clinical context and further tests are required for thorough comparison of the dosimetry parameters.[48,62] Overall, considering the linear regression analysis with erythema and AUC of the ROC analysis, the AFPM was a better dosimetry
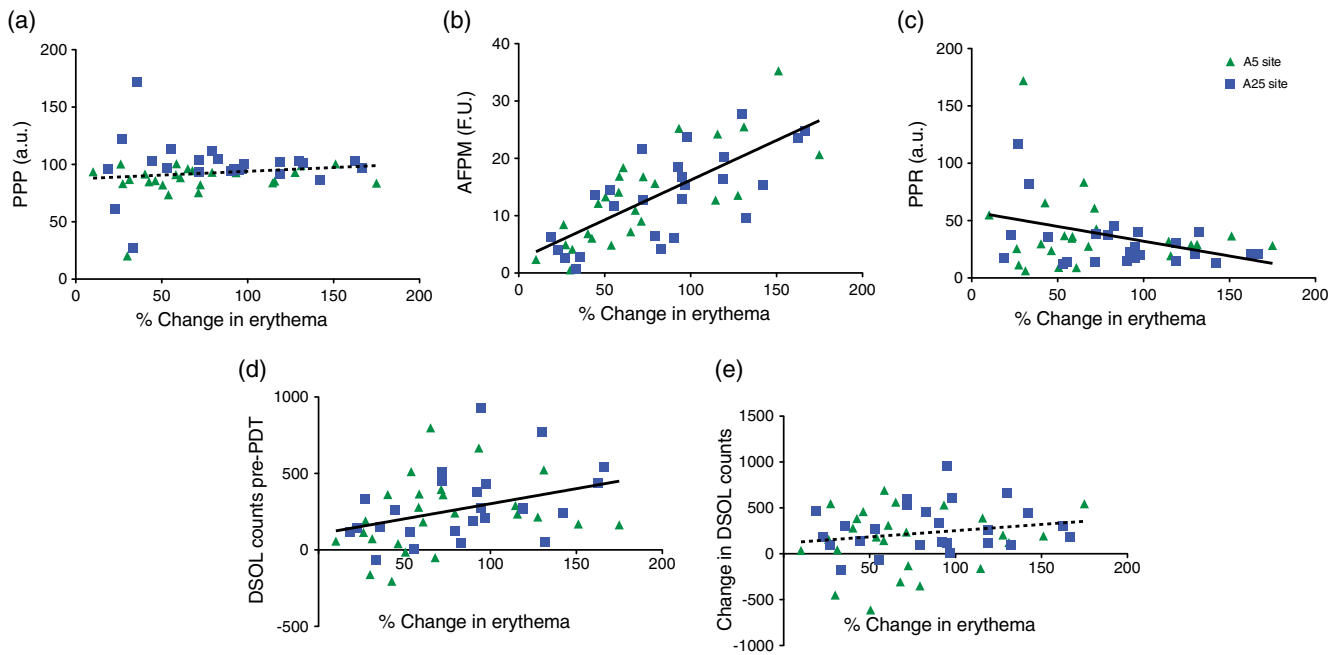
Fig. 8 Relationship between PS-Fluorescence or DSOL-based metrics and PDT-induced clinical erythema. Scatter plots illustrating the relationship between percent change in erythema and (a) % PpIX photobleached post-PDT (PPP), (b) AFPM, (c) %PpIX re-accumulation post-PDT (PPR), (d) DSOL counts pre-PDT, and (e) change in DSOL counts pre/post PDT, for the A5 (green triangles) and the A25 (blue squares) sites ($n = 25$ subjects). Each data point on the graph represents a test site. Solid black lines indicate significant, non-zero, linear regression fits with r^2 values 0.1, 0.545, and 0.13 ($p < 0.05$) for the PPR, AFPM, and DSOL counts post-PDT parameters. Parameters PPP and change in DSOL counts did not show significant correlation with percent change in erythema ($p > 0.1$). F.U. stands for fluorescence units.

parameter than DSOL counts pre-PDT and if the goal of the clinician is to correctly identify ALA-PDT nonresponding subjects, AFPM parameter will provide the results with 100% specificity (i.e., no false positive cases).

We further explored if the combination of AFPM and DSOL counts pre-PDT parameters, two mechanistically distinct dosimetry techniques, could yield better performance than either of the techniques alone. The combination of the parameters was tested using two methods: (1) Both tests are positive, i.e., a subject is treated as responder only if both AFPM and DSOL counts

pre-PDT identify the subject as a responder and (2) Either of the tests is positive, i.e., a subject is treated as responder if either of the parameters, AFPM or DSOL counts pre-PDT, identify the subject as responder. In case of "either positive" rule, the combination of the AFPM and DSOL counts pre-PDT parameters yielded a 0.77 AUC (82.05% sensitivity and 72.2% specificity), while the "both positive" rule yielded 0.79 AUC (59% sensitivity and 100% specificity). The combination of the tests using "either positive" or "both positive" rule yielded higher AUC than the DSOL counts pre-PDT parameter alone (Table 3), however, the AUC was not as good as the AFPM parameter within the context of the current study on healthy skin. Though the sensitivity increased in the "either test is positive" case, a loss of specificity was observed. As noted by Tang et al.,[63] a combination of tests always demonstrates a loss in either specificity or sensitivity when compared to the component tests alone. It
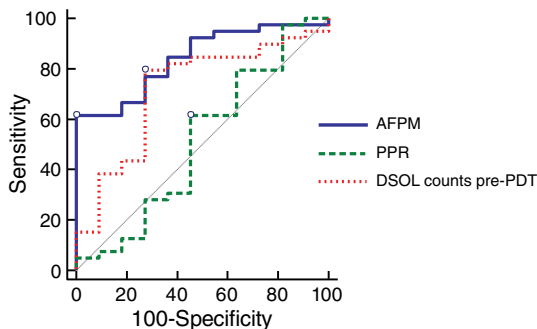
Fig. 9 PpIX fluorescence-based metrics and DSOL-based dosimetric parameters as predictors of PDT induced erythema. Receiver operating characteristic curves are plotted for AFPM (solid blue line), percent PpIX re-accumulation post-PDT PPR (dotted red line), and DSOL counts pre-PDT (dashed green line). AFPM exhibited the highest area-under-curve (AUC) of all dosimetric parameters tested. The black line indicates a reference AUC of 0.5.

Table 2 Area under the curve (AUC) statistics generated from receiver operating characteristic (ROC) curve analyses of each dosimetric parameter evaluated in the study. $N = 25$ subjects for each parameter.

Dosimetric Parameter	Area Under Curve	Standard Error	95% Confidence Interval
AFPM	0.84	0.06	0.72–0.96
PPR	0.51	0.11	0.29–0.74
DSOL counts pre-PDT	0.72	0.09	0.54–0.9

Table 3 The best cut-off for distinguishing the responders from the nonresponders was identified (i.e., maximum separation between the false positives and false negatives) is determined for AFPM and DSOLcounts pre-PDT parameters using ROC Curve analysis with Youden's index maximization. At the cut off, AUC, Sensitivity and specificity were calculated. The combination of the two parameters was tested using two methods 1. Both tests are positive, (ie., a subject is treated as responder only if both AFPM and DSOL counts pre-PDT identify the subject as responder) and 2. Either of the tests is positive (i.e., a subject is treated as responder when either AFPM or DSOL counts pre-PDT identify the subject as responder). Though the combination of the tests using "either positive" or "both positive" rule yielded higher AUC than the DSOL counts pre-PDT parameter, they were not as good as the AFPM parameter in the current study on healthy skin. CI stands for confidence interval.

	AFPM	DSOL counts pre-PDT	Both tests are positive	Either test is positive
AUC (95% CI)	0.84 (0.72–0.96)	0.72 (0.54–0.9)	0.79 (0.72–0.87)	0.774 (0.62–0.92)
Sensitivity (95% CI)	61.5 (44.6–76.6)	79.5 (63.5–90.7)	59 (42.1–74.4)	82.05 (66.5–92.5)
Specificity (95% CI)	100 (71.5–100)	72.7 (39–94)	100 (71.5–100)	72.7 (39–94)

should be noted that the sensitivity and specificity values calculated here were obtained on measurements from treatment on healthy skin. The cutoff values calculated by Youden's index maximization could change with the instrumentation or disease conditions and hence further studies in various types of skin lesions and conditions are required to thoroughly evaluate and compare the dosimetry parameters.

The PS fluorescence-based dosimetry can be easily implemented in clinical settings, although it only indicates the proportion of PS at the measurement site that emits fluorescent photons, and does not necessarily report the active PS that contributes to the therapeutic effect.[2,10,11,29–31] Furthermore, the PS fluorescence emission is dependent on various factors such as its location and interactions within the cellular microenvironment, aggregation states, and photoproduct formation.[2,25,27] In addition, the PS fluorescence is prone to various fluctuations such as those derived from PS self-shielding[12] and changes in tissue optical properties resulting from treatment.[64] As a result, the PS fluorescence-based metrics may only provide a limited representation of the deposited PDT dose. In recognition of this, accurate and direct monitoring of SOL could potentially provide a useful dosimetric measure because $^1O_2$ is thought to be an important mediator of cytotoxicity resulting from PDT.[2,11] Assuming $^1O_2$ is the only key species responsible for PDT, direct measure of SOL, preferably on-line, could be the most robust metric for PDT dosimetry. Indeed, real-time SOL detection has shown promise in pre-clinical studies, and instrumentation suitable for clinical use is still in development.[12,34,35,37,39] Thus far, only discrete measurements of SOL (DSOL), which reflect the active PS available to confer $^1O_2$ mediated cytotoxicity, have been demonstrated in human subjects.[18]

Our study primarily focuses on direct comparison of currently available clinically relevant dosimetry machines to understand which of the dose-metrics can reliably predict responders from nonresponders of the ALA-PDT treatment. Both the PpIX fluorescence and DSOL measurement systems used in our study provide point measurements and do not provide spectral data in a wide range of wavelengths. It should be noted that PpIX fluorescence measurements and DSOL measurements were performed with different excitation wavelengths (405 and 635 nm, respectively). The penetration depth in the skin of these two wavelengths is different. However, a recent study by Liu et al.[57,65] has shown that singlet oxygen generated in the fluence range used in this study is wavelength independent up to 1 mm in healthy human skin. Though the light penetration depth is different for the 405- and 635-nm excitation light, factors

such as the PS photobleaching and tissue oxygen depletion in upper dermis compensate for the variation in light distribution and generation of singlet oxygen.[57] Furthermore, the fluorescence measurement probe used in this study is designed to probe small areas that obtain data from the first 200 μm of the skin as previously demonstrated by Pogue et al.[28,41,44] Any changes in fluorescence due to change in tissue optical properties caused (due to erythema and edema in the dermis) cannot be discriminated with the fluorescence probe used in this study. In addition, the presence of water due to edema post PDT could affect the DSOL counts. However, it should be noted that singlet oxygen will be generated only at the depth[12,58,66] reachable by the excitation wavelength (635 nm). Recent studies showed that the majority of the $^1O_2$ production is at the skin surface due (1) higher accumulation of PpIX in the epidermis than the dermis and (2) availability of oxygen from the environment in the epidermis.[57,58,65] The SOL generated in the deeper dermis layers probably is not being detected by our system (edema or no edema) as the SOL signal is weak and has high reactivity of $^1O_2$ in vivo.[67] In the current study, we compared the dosimetry parameters without any compensation for difference in optical penetration depth and tissue optical properties at different excitation wavelengths. Although this is clinically relevant, it still remains that scientific analysis of the influence of tissue optical properties could show a difference in outcome. However, in this particular study it was chosen to focus on the practical clinical evaluation of the dosimetry methods rather than include tissue optical modeling as part of the analysis. In future studies, a good design would be to incorporate direct measurement of skin parameters to help evaluate the PDT dosimetry parameters.

In general, $^1O_2$ measurements, including those taken in the present study, are inherently dependent on the availability of oxygen at the measurement site.[12] Numerous studies have reported that hypoxic conditions can form a key barrier to $^1O_2$-based measurements due to sensitivity issues.[13,68,69] Pogue et al.[70] demonstrated that ALA-PDT at an irradiance of 200 mW/cm^2 and fluence of 144 J/cm^2 actually increased tissue pO$_2$ in subcutaneous RIF-1 tumors. Hypoxia due to vascular effects in PDT and its contribution to the long-term tumor response are controversial and has been studied by several groups. For example, a study by Seshadri et al.[71] showed that the ALA-PDT causes nonvascular mediated response, while the study by Becker et al.[72] showed a change in blood flow during the ALA-PDT. Mathematical simulation studies by Liu et al.[57] showed that the clinical data fit the simulation data only when the vascular oxygen supply was reduced in the

mathematical model, and this is especially true at higher radiant exposures. As shown in several studies, the PpIX primarily accumulates in the epidermis, sebaceous glands, and hair follicles in healthy human skin.[73–78] Liu et al. considered both exponential and step distribution of PpIX in the skin as a function of depth. Despite the simplification of heterogeneous distribution of PpIX in skin, the simulations by Liu et al.[57] showed that the PDT process is never oxygen limited and the majority of the singlet oxygen generated is at the epidermis (superficial layers) of the skin (0 to 0.2 mm). The study also showed that vascular changes and relevant hypoxia, due to PDT in healthy skin, are observed at depths between 0.2 and 1 mm.[57,58,66] The dermis layer beyond 1.0 mm has sufficient oxygen supply during ALA-PDT. Liu et al. also showed that the distributions of singlet oxygen are not very sensitive to the oxygen perfusion changes under a wide range of conditions. Despite the opposing conclusions from the *in vivo* tumor studies and the simulation studies, a common inference amongst these studies involving topical ALA-PDT of skin is that the majority of the singlet oxygen measurements are obtained from the superficial epidermis layer that has a constant supply of oxygen due to diffusion from surrounding air. Given these inferences, our study assumed that hypoxia was unlikely during the measurements and hypoxia had no effect on DSOL measurements."

The utility of real-time $^1O_2$-based dosimetric instrumentation currently in development remains to be tested in clinical contexts, and may suffer from the inability to report damage incurred by oxygen–independent pathways.[19,36,37,79–81] In addition, spatial tissue and the PS distribution heterogeneity in lesions will remain a challenge. As a result, more sophisticated imaging systems are being developed to obtain spatial maps of PpIX fluorescence and SOL in the region of interest simultaneously, and will hopefully address limitations inherent to point-measurement systems.[40,82]

4 Conclusions

The ALA-PDT optimization strategies that aim to maximize therapeutic efficacy, such as altering light parameters[64] or adjusting ALA administration routes,[2,83] are being actively investigated.[5,84,85] Despite these developments, the PDT outcome durability and reproducibility are challenges being addressed through several approaches, including the development of robust dosimetric methodologies. Several preclinical studies have demonstrated that high variation in PDT outcomes can be addressed by implementing dosimetric measures to guide PDT delivery.[17,39] Although various parameters have been investigated, few clinical trials currently incorporate dosimetry.[12,23,80,86–89] The present report is a first clinical investigation comparing the prognostic utility of discrete PS fluorescence-based dosimetry to discrete SOL-based dosimetry in ALA-PDT using currently available clinically relevant dosimetry machines. The findings indicate that:

i. The AFPM, had a better performance as a dosimetry parameter than other fluorescence metrics (PPP and PPR) in classifying responders from nonresponders.

ii. The DSOL counts pre-PDT had better AUC and correlation with erythema than the change in DSOL counts pre/post-PDT parameter.

iii. The AFPM had the best performance (highest AUC) in the ROC analysis among the dosimetric parameters.

iv. While DSOL-based dosimetry correlated with phototoxic response resulting from clinical ALA-PDT and had higher sensitivity, discrete PS fluorescence-based AFPM parameter had overall better performance and specificity in predicting responders from nonresponders.

v. The combination of the AFPM and DSOL counts pre-PDT metrics did not have better performance compared to AFPM alone.

With the current state of available technology, the PS fluorescence-based metrics may represent an easily implementable approach to monitor the deposited PDT dose, and could transparently be incorporated into clinical PDT regimens. With the development of efficient DSOL detection systems, further statistically rigorous studies should be conducted in various skin lesions to validate the advantage PS fluorescence-based parameters over DSOL-based parameters.

References

1. C. Clark et al., "The characteristics of erythema induced by topical 5-aminolaevulinic acid photodynamic therapy," *Photodermatol. Photoimmunol. Photomed.* **20**(2), 105–107 (2004).
2. J. P. Celli et al., "Imaging and photodynamic therapy: mechanisms, monitoring, and optimization," *Chem. Rev.* **110**(5), 2795–2838 (2010).
3. R. C. C. Brooke et al., "Histamine is released following aminolevulinic acid-photodynamic therapy of human skin and mediates an aminolevulinic acid dose-related immediate inflammatory response," *J. Invest. Dermatol.* **126**(10), 2296–2301 (2006).
4. P. G. P. Calzavara-Pinton, M. M. Venturini, and R. R. Sala, "Photodynamic therapy: update 2006. Part 2: Clinical results," *J. Eur. Acad. Dermatol. Venereol.* **21**(4), 439–451 (2007).
5. D. J. Touma and B. A. Gilchrest, "Topical photodynamic therapy: a new tool in cosmetic dermatology," *Semin. Cutaneous Med. Surg.* **22**(2), 124–130 (2003)..
6. K. A. Salva, "Photodynamic therapy: unapproved uses, dosages, or indications," *Clin. dermatol.* **20**(5), 571–581 (2002)..
7. F. H. Sakamoto, J. D. Lopes, and R. R. Anderson, "Photodynamic therapy for acne vulgaris: a critical review from basics to clinical

practice: part I. Acne vulgaris: when and why consider photodynamic therapy?," *J. Am. Acad. Dermatol.* **63**(2), 183–193 (2010).

8. M. N. Taylor and M. L. Gonzalez, "The practicalities of photodynamic therapy in acne vulgaris," *Br. J. Dermatol.* **160**(6), 1140–1148 (2009).

9. S. S. Stylli and A. H. Kaye, "Photodynamic therapy of cerebral glioma – A review Part II – Clinical studies," *J. Clinical Neurosci.* **13**(7), 709–717 (2006).

10. T. Hasan et al., "Photodynamic therapy of cancer," in *Holland-Frei Cancer Medicine*, D. Kute et al., Eds., p. 605422, Dekker Inc., Hamilton, Canada (2003).

11. B. C. Wilson and M. S. Patterson, "The physics, biophysics and technology of photodynamic therapy," *Phys. Med. Biol.* **53**(9), R61–R109 (2008).

12. B. C. Wilson, M. S. Patterson, and L. Lilge, "Implicit and explicit dosimetry in photodynamic therapy: a New paradigm," *Lasers Med. Sci.* **12**(3), 182–199 (1997).

13. M. T. Jarvi et al., "Singlet oxygen luminescence dosimetry (SOLD) for photodynamic therapy: current status, challenges and future prospects," *Photochem. Photobiol.* **82**(5), 1198–1210 (2006).

14. W. M. Star et al., "Quantitative model calculation of the time-dependent protoporphyrin IX concentration in normal human epidermis after delivery of ALA by passive topical application or iontophoresis," *Photochem. Photobiol.* **75**(4), 424–432 (2002).

15. H. S. H. de Bruijn et al., "Increase in protoporphyrin IX after 5-aminolevulinic acid based photodynamic therapy is due to local re-synthesis," *Photochem. Photobiol. Sci.* **6**(8), 857–864 (2007).

16. M. S. Patterson and E. Mazurek, "Calculation of cellular oxygen concentration for photodynamic therapy in vitro," *Methods Mol. Biol.* **635**, 195–205 (2010).

17. T. C. Zhu and J. C. Finlay, "Prostate PDT dosimetry," *Photodiagn. Photodyn. Ther.* **3**(4), 234–246 (2006).

18. H.-J. Laubach et al., "In-vivo singlet oxygen dosimetry of clinical 5-aminolevulinic acid photodynamic therapy," *J. Biomed. Opt.* **13**(5), 050504 (2008).

19. B. W. Pogue et al., "Fluorescent molecular imaging and dosimetry tools in photodynamic therapy," *Methods Mol. Biol.* **635**, 207–222 (2010).

20. M. R. Thissen et al., "PpIX fluorescence kinetics and increased skin damage after intracutaneous injection of 5-aminolevulinic acid and repeated illumination," *J. Invest. Dermatol.* **118**(2), 239–245 (2002).

21. D. J. Robinson et al., "Fluorescence photobleaching of ALA-induced protoporphyrin IX during photodynamic therapy of normal hairless mouse skin: the effect of light dose and irradiance and the resulting biological effect," *Photochem. Photobiol.* **67**(1), 140–149 (1998).

22. M. A. Weston and M. S. Patterson, "Calculation of singlet oxygen dose using explicit and implicit dose metrics during benzoporphyrin derivative monoacid ring A (BPD-MA)-PDT in vitro and correlation with MLL cell survival," *Photochem. Photobiol.* **87**(5), 1129–1137 (2011).

23. I. A. I. Boere et al., "Monitoring in situ dosimetry and protoporphyrin IX fluorescence photobleaching in the normal rat esophagus during 5-aminolevulinic acid photodynamic therapy," *Photochem. Photobiol.* **78**(3), 271–277 (2003).

24. X. Zhou et al., "Pretreatment photosensitizer dosimetry reduces variation in tumor response," *Radiat. Oncol. Biol.* **64**(4), 1211–1220 (2006).

25. J. S. Dysart and M. S. Patterson, "Photobleaching kinetics, photoproduct formation, and dose estimation during ALA induced PpIX PDT of MLL cells under well oxygenated and hypoxic conditions," *Photochem. Photobiol. Sci.* **5**(1), 73–81 (2006).

26. C. C. Lee et al., "Spatial heterogeneity and temporal kinetics of photosensitizer (AlPcS2) concentration in murine tumors RIF-1 and MTG-B," *Photochem. Photobiol. Sci.* **2**(2), 145–150 (2003).

27. I. Georgakoudi and T. H. Foster, "Singlet oxygen-versus nonsinglet oxygen-mediated mechanisms of sensitizer photobleaching and their effects on photodynamic dosimetry," *Photochem. Photobiol.* **67**(6), 612–625 (1998).

28. B. W. Pogue and G. Burke, "Fiber-optic bundle design for quantitative fluorescence measurement from tissue," *Appl. Opt.* **37**(31), 7429–7436 (1998).

29. Z. Ji et al., "Subcellular localization pattern of protoporphyrin IX is an important determinant for its photodynamic efficiency of human carcinoma and normal cell lines," *J. Photochem. Photobiol. B: Biol.* **84**(3), 213–220 (2006).

30. J. J. Morgan and A. R. A. Oseroff, "Mitochondria-based photodynamic anti-cancer therapy," *Adv. Drug Delivery Rev.* **49**(1–2), 16–16 (2001).

31. I. J. MacDonald et al., "Subcellular localization patterns and their relationship to photodynamic activity of pyropheophorbide-a derivatives," *Photochem. Photobiol.* **70**(5), 789–797 (1999).

32. J. C. Finlay et al., "Photobleaching kinetics of Photofrin in vivo and in multicell tumour spheroids indicate two simultaneous bleaching mechanisms," *Phys. Med. Biol.* **49**(21), 4837–4860 (2004).

33. I. Rizvi et al., "PDT dose parameters impact tumoricidal durability and cell death pathways in a 3D ovarian cancer model," *Photochem. Photobiol.* **89**(4), 942–952 (2013).

34. M. J. Niedre et al., "Singlet oxygen luminescence as an in vivo photodynamic therapy dose metric: validation in normal mouse skin with topical amino-levulinic acid," *Br. J. Cancer* **92**(2), 298–304 (2005).

35. J. Yamamoto et al., "Monitoring of singlet oxygen is useful for predicting the photodynamic effects in the treatment for experimental glioma," *Clin. Cancer Res.* **12**(23), 7132–7139 (2006).

36. S. Lee et al., "Pulsed diode laser-based monitor for singlet molecular oxygen," *J. Biomed. Opt.* **13**(3), 034010 (2008).

37. J. Baier et al., "Direct detection of singlet oxygen generated by UVA irradiation in human cells and skin," *J. Invest. Dermatol.* **127**(6), 1498–1506 (2007).

38. T. B. Fitzpatrick, "The validity and practicality of sun-reactive skin types I through VI," *Arch. Dermatol.* **124**(6), 869 (1988).

39. S. Lee et al., "Pulsed diode laser-based singlet oxygen monitor for photodynamic therapy: in vivo studies of tumor-laden rats," *J. Biomed. Opt.* **13**(6), 064035 (2008).

40. S. Lee et al., "Dual-channel imaging system for singlet oxygen and photosensitizer for PDT," *Biomed. Opt. Express* **2**(5), 1233–1242 (2011).

41. C. C. Lee et al., "Comparison of photosensitizer (AIPcS2) quantification techniques: in situ fluorescence microsampling versus tissue chemical extraction," *Photochem. Photobiol.* **74**(3), 453–460 (2001).

42. C. B. Warren et al., "Noninvasive fluorescence monitoring of protoporphyrin IX production and clinical outcomes in actinic keratoses following short-contact application of 5-aminolevulinate," *J. Biomed. Opt.* **15**(5), 051607 (2010).

43. B. W. Pogue et al., "Protoporphyrin IX fluorescence photobleaching increases with the use of fractionated irradiation in the esophagus," *J. Biomed. Opt.* **13**(3), 034009 (2008).

44. B. W. Pogue et al., "Analysis of sampling volume and tissue heterogeneity on the in vivo detection of fluorescence," *J. Biomed. Opt.* **10**(4), 041206 (2005).

45. H. Zeng et al., "Monitoring photoproduct formation and photobleaching by fluorescence spectroscopy has the potential to improve PDT dosimetry with a verteporfin-like photosensitizer," *Photochem. Photobiol.* **75**(4), 398–405 (2002).

46. M. A. V. Santos, V. G. Belo, and G. Santos, "Effectiveness of photodynamic therapy with topical 5-aminolevulinic acid and intense pulsed light versus intense pulsed light alone in the treatment of acne vulgaris: comparative study," *Dermatol. Surg.* **31**(8 Pt 1), 910–915 (2005).

47. E. R. DeLong, D. M. DeLong, and D. L. Clarke-Pearson, "Comparing the areas under two or more correlated receiver operating characteristic curves: a nonparametric approach," *Biometrics* **44**(3), 837–845 (1988).

48. E. F. Schisterman et al., "Optimal cut-point and its corresponding youden index to discriminate individuals using pooled blood samples," *Epidemiology* **16**(1), 73–81 (2005).

49. S. S. Fabricius et al., "The relation between methyl aminolevulinate concentration and inflammation after photodynamic therapy in healthy volunteers," *Photochem. Photobiol. Sci.* **12**(1), 117–123 (2012).

50. M. A. Pathak and J. W. Burnett, "The porphyrin content of skin," *J. Invest. Dermatol.* **43**, 119–120 (1964).

51. I. Seo et al., "Fluorescence spectroscopy for endogenous porphyrins in human facial skin," *Proc. SPIE* **7161**, 716103 (2009).

52. F. Leblond et al., "Pre-clinical whole-body fluorescence imaging: Review of instruments, methods and applications," *J. Photochem. Photobiol. B: Biol.* **98**(1), 77–94 (2010).

53. J. S. Tyrrell, S. M. Campbell, and A. Curnow, "The relationship between protoporphyrin IX photobleaching during real-time dermatological methyl-aminolevulinate photodynamic therapy (MAL-PDT) and subsequent clinical outcome," *Lasers Surg. Med.* **42**(7), 613–619 (2010).

54. C. Sheng et al., "Photobleaching-based dosimetry predicts deposited dose in ALA-PpIX PDT of rodent esophagus," *Photochem. Photobiol.* **83**(3), 738–748 (2007).

55. W. J. Cottrell et al., "Irradiance-dependent photobleaching and pain in -aminolevulinic acid-photodynamic therapy of superficial basal cell carcinomas," *Clin. Cancer Res.* **14**(14), 4475–4483 (2008).

56. J. Tyrrell, S. Campbell, and A. Curnow, "Protoporphyrin IX photobleaching during the light irradiation phase of standard dermatological methyl-aminolevulinate photodynamic therapy," *Photodiagn. Photodyn. Ther.* **7**(4), 232–238 (2010)

57. B. Liu, T. J. Farrell, and M. S. Patterson, "Comparison of noninvasive photodynamic therapy dosimetry methods using a dynamic model of ALA-PDT of human skin," *Phys. Med. Biol.* **57**(3), 825–841 (2012).

58. B. Liu, T. J. Farrell, and M. S. Patterson, "A dynamic model for ALA-PDT of skin: simulation of temporal and spatial distributions of ground-state oxygen, photosensitizer and singlet oxygen," *Phys. Med. Biol.* **55**(19), 5913–5932 (2010).

59. B. Liu, "Comparison of photodynamic therapy with different excitation wavelengths using a dynamic model of aminolevulinic acid-photodynamic therapy of human skin," *J. Biomed. Opt.* **17**(8), 088001 (2012).

60. J. S. Dysart, G. Singh, and M. S. Patterson, "Calculation of singlet oxygen dose from photosensitizer fluorescence and photobleaching during mTHPC photodynamic therapy of MLL cells," *Photochem. Photobiol.* **81**(1), 196–205 (2005).

61. E. F. Schisterman et al., "Optimal cut-point and its corresponding Youden Index to discriminate individuals using pooled blood samples," *Epidemiology* **16**(1), 73–81 (2005).

62. M. H. Zweig and G. Campbell, "Receiver-operating characteristic (ROC) plots: a fundamental evaluation tool in clinical medicine," *Clin. Chem.* **39**(4), 561–577 (1993).

63. M.-L. M. Tang, "On simultaneous assessment of sensitivity and specificity when combining two diagnostic tests," *Stat. Med.* **23**(23), 3593–3605 (2004).

64. S. L. Jacques, "How tissue optics affect dosimetry of photodynamic therapy," *J. Biomed. Opt.* **15**(5), 051608 (2010).

65. B. Liu, "Comparison of photodynamic therapy with different excitation wavelengths using a dynamic model of aminolevulinic acid-photodynamic therapy of human skin," *J. Biomed. Opt.* **17**(8), 088001 (2012).

66. K. K.-H. Wang et al., "Simulations of measured photobleaching kinetics in human basal cell carcinomas suggest blood flow reductions during ALA-PDT," *Lasers Surg. Med.* **41**(9), 686–696 (2009).

67. M. T. Jarvi et al., "Insights into photodynamic therapy dosimetry: simultaneous singlet oxygen luminescence and photosensitizer photobleaching measurements," *Biophys. J.* **102**(3), 661–671 (2012).

68. S. Oelckers et al., "Time-resolved detection of singlet oxygen luminescence in red-cell ghost suspensions: concerning a signal component that can be attributed to 1O2 luminescence from the inside of a native membrane," *J. Photochem. Photobiol., B: Biol.* **53**(1–3), 121–127 (1999).

69. I. Georgakoudi, P. C. Keng, and T. H. Foster, "Hypoxia significantly reduces aminolaevulinic acid-induced protoporphyrin IX synthesis in EMT6 cells," *Br. J. Cancer* **79**(9–10), 1372–1377 (1999).

70. B. W. Pogue et al., "Tumor PO(2) changes during photodynamic therapy depend upon photosensitizer type and time after injection," *Comp. Biochem. Physiol., Part A Mol. Integr. Physiol.* **132**(1), 177–184 (2002).

71. M. Seshadri et al., "Tumor vascular response to photodynamic therapy and the antivascular agent 5,6-dimethylxanthenone-4-acetic acid: implications for combination therapy," *Clin. Cancer Res.* **11**(11), 4241–4250 (2005).

72. T. L. Becker et al., "Monitoring blood flow responses during topical ALA-PDT," *Biomed. Opt. Express* **2**(1), 123–130 (2011).

73. E. R. de Haas et al., "Microscopic distribution of protoporphyrin (PpIX) fluorescence in superficial basal cell carcinoma during light-fractionated aminolaevulinic acid photodynamic therapy," *Acta Derm. Venereol.* **88**(6), 547–554 (2008).

74. J. T. van den Akker et al., "Protoporphyrin IX fluorescence kinetics and localization after topical application of ALA pentyl ester and ALA on hairless mouse skin with UVB-induced early skin cancer," *Photochem. Photobiol.* **72**(3), 399–406 (2000).

75. H. S. de Bruijn et al., "Microscopic localisation of protoporphyrin IX in normal mouse skin after topical application of 5-aminolevulinic acid or methyl 5-aminolevulinate," *J. Photochem. Photobiol. B: Biol.* **92**(2), 91–97 (2008).

76. F. H. Sakamoto et al., "Intracutaneous ALA photodynamic therapy: dose-dependent targeting of skin structures," *Lasers Surg. Med.* **43**(7), 621–631 (2011).

77. N. Dögnitz et al., "Comparison of ALA- and ALA hexyl-ester-induced PpIX depth distribution in human skin carcinoma," *J. Photochem. Photobiol., B: Biol.* **93**(3), 140–148 (2008).

78. N. N. van der Veen et al., "Kinetics and localisation of PpIX fluorescence after topical and systemic ALA application, observed in skin and skin tumours of UVB-treated mice," *Br. J. Cancer* **73**(7), 925–930 (1996).

79. Y. Wang et al., "Fluorescence monitoring of a photosensitizer and prediction of the therapeutic effect of photodynamic therapy for port wine stains," *Exp. Biol. Med.* **235**(2), 175–180 (2010)..

80. W. J. Cottrell, A. R. Oseroff, and T. H. Foster, "Portable instrument that integrates irradiation with fluorescence and reflectance spectroscopies during clinical photodynamic therapy of cutaneous disease," *Rev. Sci. Instrum.* **77**(6), 064302 (2006).

81. M. M. Niedre, M. S. M. Patterson, and B. C. B. Wilson, "Direct near-infrared luminescence detection of singlet oxygen generated by photodynamic therapy in cells in vitro and tissues in vivo," *Photochem. Photobiol.* **75**(4), 382–391 (2002).

82. N. R. Gemmell et al., "Singlet oxygen luminescence detection with a fiber-coupled superconducting nanowire single-photon detector," *Opt. Express* **21**(4), 5005–5013 (2013).

83. R. Lopez, "Photodynamic therapy of skin cancer: controlled drug delivery of 5-ALA and its esters," *Adv. Drug Delivery Rev.* **56**(1), 77–94 (2004).

84. M. H. Gold and M. P. Goldman, "5-aminolevulinic acid photodynamic therapy: where we have been and where we are going," *Dermatol. Surg.* **30**(8), 1077–1083 (2004).

85. W. Hongcharu et al., "Topical ALA-photodynamic therapy for the treatment of acne vulgaris," *J. Invest. Dermatol.* **115**(2), 183–192 (2000).

86. F. H. Sakamoto, L. Torezan, and R. R. Anderson, "Photodynamic therapy for acne vulgaris: a critical review from basics to clinical practice: Part II. Understanding parameters for acne treatment with photodynamic therapy," *J. Am. Acad. Dermatol.* **63**(2), 195–211 (2010).

87. W. Sharman, C. Allen, and J. E. van Lier, "Photodynamic therapeutics: basic principles and clinical applications," *Drug Discovery Today* **4**(11), 507–517 (1999).

88. F. S. De Rosa and M. V. Bentley, "Photodynamic therapy of skin cancers: sensitizers, clinical studies and future directives," *Pharm. Res.* **17**(12), 1447–1455 (2000).

89. J. Tyrrell, S. M. Campbell, and P. A. Curnow, "Monitoring the accumulation and dissipation of the photosensitizer protoporphyrin IX during standard dermatological methyl-aminolevulinate photodynamic therapy utilizing non-invasive fluorescence imaging and quantification," *Photodiagn. Photodyn. Ther.* **8**(1), 30–38 (2011).

Biographies of the authors are not available.